

ENVIRONMENTAL STUDIES

Uncovering the impacts of depleting aquifers: A remote sensing analysis of land subsidence in Iran

Mahmud Haghshenas Haghghi^{1,*} and Mahdi Motagh^{2,1}

Intensive groundwater pumping, previously unrecognized in its full extent, is blamed for aquifer degradation and widespread land subsidence in Iran. We use a 100-meter resolution satellite survey from 2014 to 2020 to assess the recent implications of groundwater usage across the country. Results indicate that approximately 56,000 km² (3.5%) of the country's area is subject to land subsidence, primarily linked to irrigation; 3000 km² of this area experiences subsidence rates greater than 10 cm/year. The central plateau catchment hosts two-thirds of the country's depleting aquifers, with locations sinking at rates higher than 35 cm/year. The results suggest an annual groundwater depletion of 1.7 billion cubic meters (BCM) from confined and semiconfined aquifers, with the long-term inelastic compaction for most aquifers being approximately one order of magnitude larger than their seasonal elastic response. This underscores the permanent loss of aquifers that jeopardizes the sustainability of water resources across Iran.

INTRODUCTION

Iran, a vast nation covering 1.6 million km² with a population of approximately 84 million, faces an impending groundwater crisis of critical proportions. The compounding factors of a quadrupled population over the past six decades, rapid industrialization, and expansive agriculture have placed immense pressure on Iran's water resources. To meet escalating demands, unsustainable groundwater extraction has become the norm, resulting in a troubling trajectory of resource depletion (1, 2). Groundwater, a lifeline for nearly a quarter of Iran's inhabitants, particularly in arid and semi-arid regions, now confronts a paradoxical challenge. The demand for groundwater surpasses its replenishment capacity, disrupting the delicate balance of the natural water cycle. This pervasive water stress not only endangers communities but also triggers ecological imbalances, necessitating urgent exploration of the multifaceted consequences of groundwater depletion.

Despite the urgent need for a comprehensive and detailed analysis of groundwater, this analysis has been lacking at a fine scale. At a large scale and with rough resolution, Iran's groundwater crisis is vividly underscored by past findings of global groundwater models or Gravity Recovery and Climate Experiment (GRACE) observations (3–5). In 2000, it was estimated that nearly half of Iran's total groundwater extraction was unsustainable (6). Furthermore, groundwater well measurements unveiled an alarming annual depletion rate of approximately 5.7 billion cubic meters (BCM) between 2002 and 2015, a phenomenon corroborated by GRACE measurements detecting water storage loss across the country (7, 8). Assimilating GRACE data into a global hydrology model further accentuated the issue, revealing a reduction of about 9 cm in groundwater levels during the decade from 2002 to 2012 (9). The staggering cumulative impact emerges in the statistic that Iran has lost approximately 211 ± 34 BCM of its total water storage over the past two decades (10).

These stark figures underline the urgent need to address Iran's groundwater dilemma comprehensively. Beyond the sheer volume of water lost, the consequences are far-reaching. Diminished groundwater resources affect agricultural productivity, threatening Iran's food

security. Industries reliant on groundwater face uncertainty and escalating costs. Furthermore, land subsidence, a direct result of excessive groundwater extraction, can damage critical infrastructure, including roads, buildings, and pipelines (11). The social and economic implications are undeniable, amplifying the urgency of understanding and mitigating this crisis.

Land subsidence is a tangible indicator of distress within Iran's aquifers. It occurs when excessive water withdrawal leads to a drop in hydraulic head, causing skeletal compaction of the soil primarily in the aquitards—the low-permeable layers composed of small grains such as clay and silt. When the hydraulic head drops below its historical level or the preconsolidation head, the compaction is inelastic and hence permanent (12). In regions heavily reliant on groundwater, such as the capital Tehran (13), the agricultural center Rafsanjan (14), and the populous city of Mashhad (15), land subsidence has become a cause for concern, signaling an underlying groundwater crisis.

In recent years, a few studies have attempted to use Interferometric Synthetic Aperture Radar (InSAR) for large-scale subsidence mapping or prediction in Iran. One such study analyzed a 3-year period of Sentinel-1 data between 2014 and 2017 to identify hot spots of subsidence across the country. The findings revealed widespread land subsidence, with rates of up to 30 cm/year in certain areas (16). Other studies integrated InSAR data into machine learning models to upscale the measurements and predict land subsidence at larger scales. One study used approximately 80 Sentinel-1 images from known subsidence areas and applied conventional InSAR analysis to form the basis of a machine-learning model to predict subsidence in various parts of the country (17). Another study used a large InSAR training dataset from various areas around the world to predict subsidence rates at a global scale. The study specifically used training data over four subsidence areas in Iran. Using a machine learning technique, it found that almost 1% of Iran's area, summing up to 18,000 km², is subsiding at rates higher than 1 cm/year, making Iran ranked fourth in terms of subsidence area in the world (18).

The main question that we aim to address in this study is: What is the exact extent of groundwater depletion in Iran and what are its implications on the groundwater resources and the communities? Our study pioneers a comprehensive analysis of Iran's groundwater dynamics through the utilization of InSAR observations. Using more than 6000 Sentinel-1 images, we have produced a subsidence map at a

Copyright © 2024 The Authors, some rights reserved; exclusive licensee American Association for the Advancement of Science. No claim to original U.S. Government Works. Distributed under a Creative Commons Attribution License 4.0 (CC BY).

¹Institute of Photogrammetry and Geoinformation, Leibniz University Hannover, Hannover, Germany. ²Helmholtz Centre Potsdam–GFZ German Research Centre for Geosciences, Potsdam, Germany.

*Corresponding author. Email: mahmud@ipi.uni-hannover.de

medium resolution of 100 m, capturing temporal variations at intervals ranging from 6 to 24 days. This extensive dataset enables us to isolate the subsidence signals from other InSAR observation contributions, providing a comprehensive subsidence mapping of the country.

Furthermore, our integration of geological information, sedimentary deposit thickness, and aquifer outlines with InSAR data provides evidence that the observed subsidence is primarily due to aquifer compaction resulting from excessive groundwater extraction. We further quantify groundwater depletion across the country from subsidence measurements and evaluate its sustainability across diverse regions by comparing long-term compaction trends with short-term deformations. Our analysis of the role of agriculture in unsustainable groundwater use, through examining land cover maps and

agricultural production data, offers an insight into the link between agricultural practices and groundwater sustainability in Iran. In addition, we explore the far-reaching implications of land subsidence on human communities and critical infrastructure; by analyzing population density data and infrastructure maps, we highlight the socioeconomic consequences of land subsidence.

RESULTS

Land subsidence and associated groundwater loss across Iran

The nationwide subsidence map (Fig. 1) illustrates the distribution and extent of land subsidence across Iran, revealing a widespread issue occurring at both local and regional levels. Approximately 3.5%

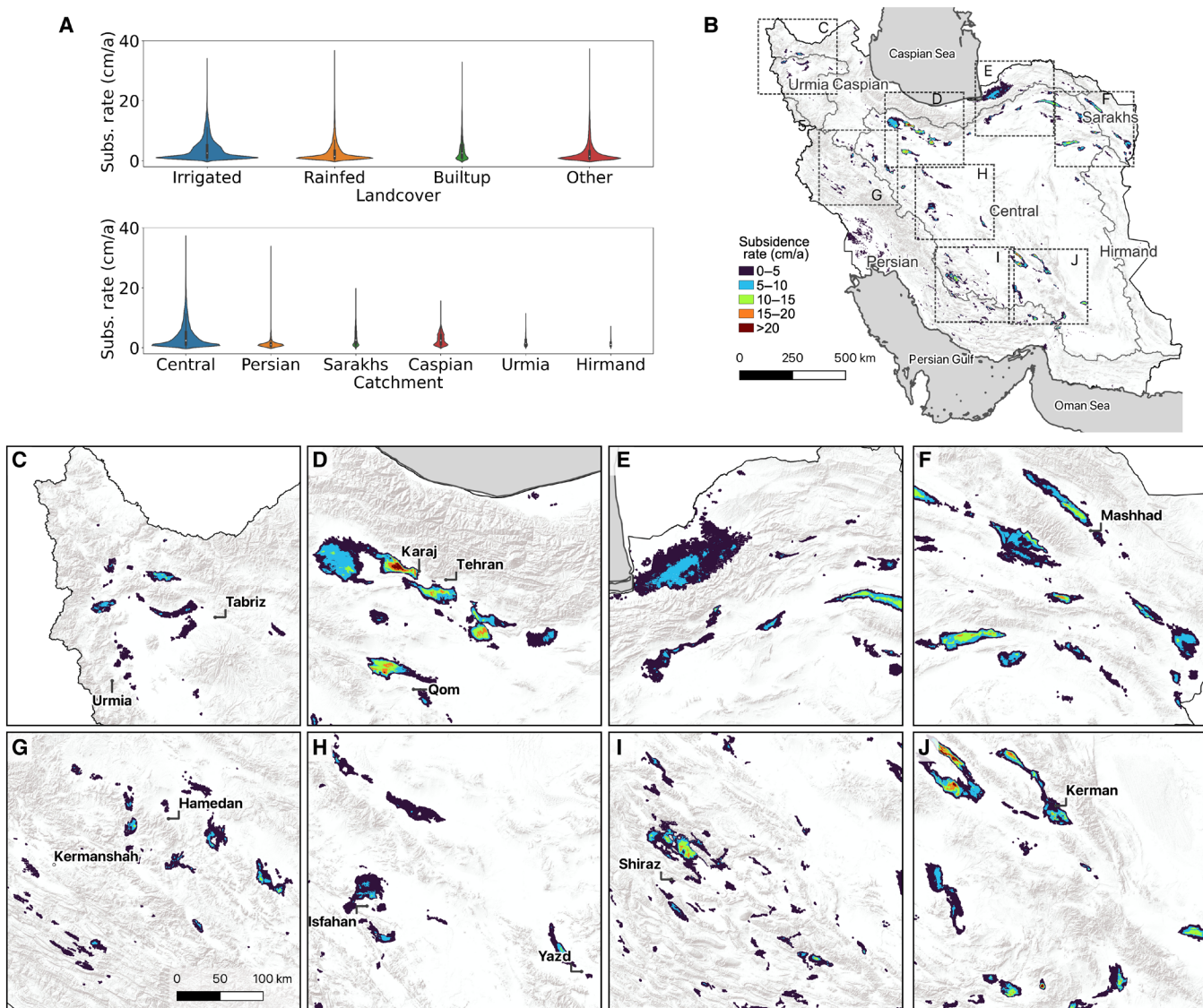


Fig. 1. Land subsidence across Iran through Sentinel-1 InSAR observation. (A) Distribution of subsidence for different land covers and across the country's six major basins. (B) Comprehensive land subsidence rate map of Iran. The lines indicate the borders of the major catchments. The boxes are intended to highlight the main areas that are affected by land subsidence, as shown in (C to J). The rates of subsidence are projected based on the satellite line-of-sight measurements under the assumption that subsidence is the primary component of surface deformation.

of Iran's land, equivalent to 56,000 km², is facing land subsidence hazard. The median value of subsidence rates from 2014 to 2020 is 1.8 cm/year. The distribution of subsidence rates is positively skewed, with quartiles at 0.9, 1.8, and 4.1 cm/year. More specifically, a combined total area over 40,000 km² is subject to subsidence rates higher than 1 cm/year, while areas amounting to more than 25,000 km² sink at rates exceeding 2 cm/year; over 3000 km² of the country is subsidizing at alarming rates greater than 10 cm/year.

To examine whether aquifer compaction is the primary reason for the observed subsidence, we performed several tests by comparing the subsidence areas with the superficial geological map of Iran (19, 20), a global 1-km gridded sedimentary deposit thickness (21), and available aquifer boundaries (22). An overlay of subsidence areas on the superficial geology map of Iran, as shown in fig. S2, shows that 80% of the measured subsidence across the country occurs in Quaternary sediments. Quaternary sediments are young geological deposits known for their unconsolidated deposits that can serve as good aquifers. In addition, overlaying the subsidence map on the map of average soil and sedimentary deposit thickness shows that 80% of the subsidence occurs in sediments with a deposit thickness greater than 25 m. Lastly, 90% of the subsidence we identified is located within aquifer boundaries. These findings are also consistent with detailed numerical modeling of subsidence performed at local scales, for example, in Rafsanjan (23). All of this evidence firmly suggests that aquifer compaction could be the main factor explaining the observed subsidence.

Our analysis reveals that land subsidence is a prevalent issue across Iran, affecting 265 of the country's 429 counties. The subsidence phenomenon extends over vast areas, with eight counties experiencing subsiding areas exceeding 1000 km². These counties include Kerman, Rafsanjan, and Sirjan in Kerman province; Marvdasht in Fars province; Neishabur in Khorasan Razavi province; Buin-Zahra in Qazvin province; and Gonbad-Kavus and Aqqala in Golestan province. Among the regions experiencing the most severe ground sinking, Kerman province stands out with alarming subsidence rates. Particularly, Rafsanjan county, known for being Iran's center of pistachio production, experiences the highest subsidence rate at an astonishing 37 cm/year. Close behind, Arzuiyeh county, also in Kerman province, records a substantial rate of 34 cm/year. In Alborz province, Savojbolagh and Nazarabad counties exhibit substantial land subsidence, with maximum rates of 29 and 27 cm/year, respectively.

We observed the presence of land subsidence in all provinces of Iran except for Gilan. The variability of subsidence across different areas is evident, particularly in the north, which receives the largest share of the country's rainfall. The absence of subsidence in Gilan indicates that the region does not heavily rely on groundwater extraction on a large scale. In contrast, Mazandaran experiences moderate land subsidence, affecting approximately 140 km² of its land with a maximum rate of 4 cm/year at some locations. Meanwhile, Golestan province faces a more notable challenge, with large land subsidence occurring over an area of more than 5000 km². In this region, subsidence rates exceed 12 cm/year at some locations.

Estimating groundwater depletion from land subsidence rates provides valuable insights into the extent of water resource utilization in each province (Fig. 2). Assuming subsidence primarily occurs in the confining parts of aquifers, we calculated the annual groundwater depletion for each region. On average, the country experiences a total yearly groundwater deficit of 1737 million cubic meters (MCM). Out of this, the provinces of Khorasan Razavi and Kerman face the most

severe water stress, depleting approximately 380 and 325 MCM of groundwater each year, respectively. Golestan province also experiences substantial depletion, accounting for around 162 MCM per year. Following closely are Fars province with 141 MCM, Qazvin with 103 MCM, and Tehran with 101 MCM of groundwater depletion annually. While still affected, the remaining provinces experience less than 100 MCM of groundwater deficit per year.

Normalizing the groundwater depletion for the area of each province reveals an additional pattern, shedding light on the intensity of water resource utilization per unit of land (Fig. 2). Karaj province ranks first on the list, with a staggering 12,800 m³ of groundwater depletion per km² each year. Golestan closely follows as the second-highest with 8000 m³/km² per year. Tehran and Qazvin provinces are next in line, both experiencing 7400 and 6600 m³ of yearly deficit per square kilometer, respectively. Khorasan Razavi and Qom provinces are the subsequent regions, facing annual depletion of 3300 and 2800 m³/km². All these provinces fall within the northern half of the country.

Analyzing the distribution of subsidence and groundwater loss at both the basin and sub-basin scales provides valuable insights into the regional variations in water resource depletion. At the basin scale, the Central Plateau basin, covering half of the country's area, emerges as the primary contributor to Iran's groundwater depletion, responsible for 70% of the total loss. Unexpectedly, despite receiving the highest precipitation rate among basins, the Caspian Sea basin ranks second, accounting for 11% of the groundwater depletion. The Persian Gulf basin follows closely as the third largest contributor, with 10% of the country's groundwater depletion, despite holding the largest share of the nation's water resources. Sarakhs basin and Urmia basin are next in line, contributing 6% and less than 2%, respectively, while the Hirmand basin's share is smaller than 1%.

Zooming into the sub-basin level, a more granular pattern emerges. Almost half of Iran's groundwater loss occurs in two sub-basins: Salt Lake and Central Desert, responsible for 23% and 20% of the total depletion, respectively. Saghond sub-basin follows closely with 11% of the groundwater loss. Other sub-basins each has a share smaller than 10%. Two sub-basins, Talesh and Sefidrud-Haraz, located in the north, do not experience any groundwater loss due to ample availability of water resources, thus they do not rely on groundwater for irrigation. In contrast, the low share of eastern sub-basins of Khaf, Hamun-Hirmand, Hamun-Mashkil, and Baluchestan is due to non-arable lands and low populations. Normalization of the data by basin area further highlights the intensity of groundwater depletion per unit of land. Gharesu-Gorgan sub-basin stands out with the largest yearly groundwater depletion per area, amounting to 11,000 m³/km². It is followed by Salt Lake, Saghond, and Tashk-Bakhtegan with annual depletions of 4300, 3700, and 3300 m³/km², respectively.

Sustainable versus unsustainable groundwater use

The surface deformation time series provides insights into the proportion of elastic and inelastic deformation. In this context, inelastic deformation refers to the long-term subsidence resulting from the permanent compaction of aquitards due to declining groundwater heads. On the other hand, elastic deformation arises from seasonal recharge cycles, causing temporary fluctuations in the aquifer system. We calculated the elastic-to-inelastic ratio by examining the peak-to-peak amplitude of subsidence as elastic and the average yearly subsidence as inelastic.

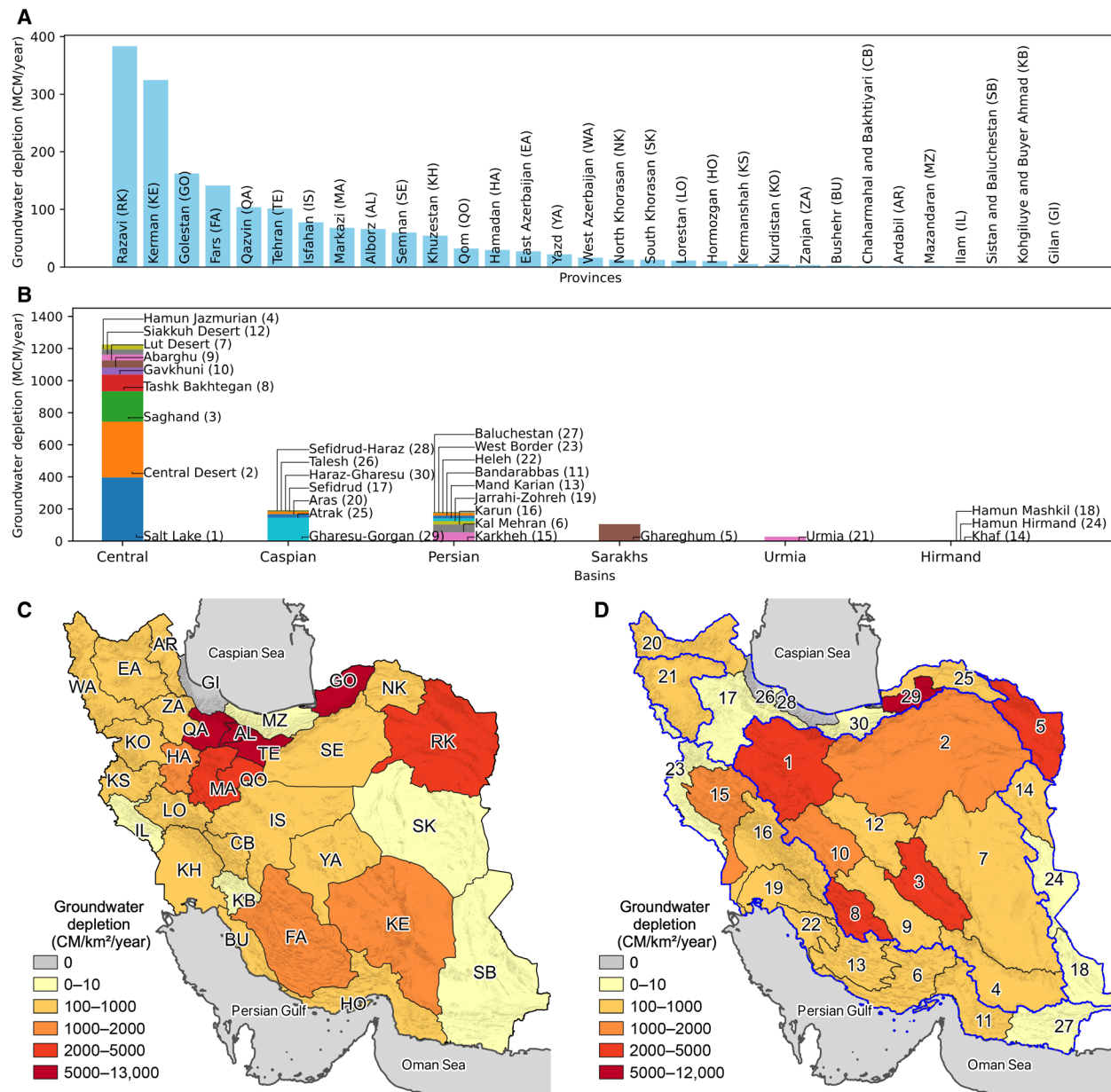


Fig. 2. Groundwater depletion from confined and semi-confined aquifers in Iran. (A) Share of each province in annual groundwater depletion. (B) Share of each basin and sub-basin in annual groundwater depletion. (C and D) Annual groundwater depletion per square kilometer in different provinces and sub-basins. The groundwater depletion is estimated using subsidence data, assuming that the compaction of confined and semi-confined parts of the aquifer system causes the dominant factor of subsidence. The province names in (C) are abbreviated for simplicity and correspond to the full names in (A). The sub-basins in (D) are numbered for simplicity and correspond to the full names in (B). Blue lines in (D) indicate the boundaries of major basins.

The time series of surface deformation for two representative points near Tehran and Karaj, as shown in Fig. 3, demonstrates that the deformation is dominated by these two components. Although both points are situated within a similar geological formation of quaternary sediments with thicknesses exceeding 50 m, the aquifer system associated with the second point shows both larger seasonal and long-term components. For the point in the subsidence area to the southwest of Tehran, we estimate an elastic/inelastic ratio of 0.1, which corresponds to a 2-cm amplitude of the seasonal deformation and an average annual

subsidence of 18 cm. For the second point, located southwest of Karaj, the elastic/inelastic ratio is 0.4, corresponding to an 11-cm seasonal component and 29 cm of annual subsidence. In a similar analysis across the country, our findings reveal that the annual compaction of most aquifers is approximately one order of magnitude larger than the seasonal elastic response of the aquifer system. Although not directly linked to the proportion of extracted groundwater, this elastic-inelastic ratio offers insights into the relative sustainability of groundwater use across different regions of the country.

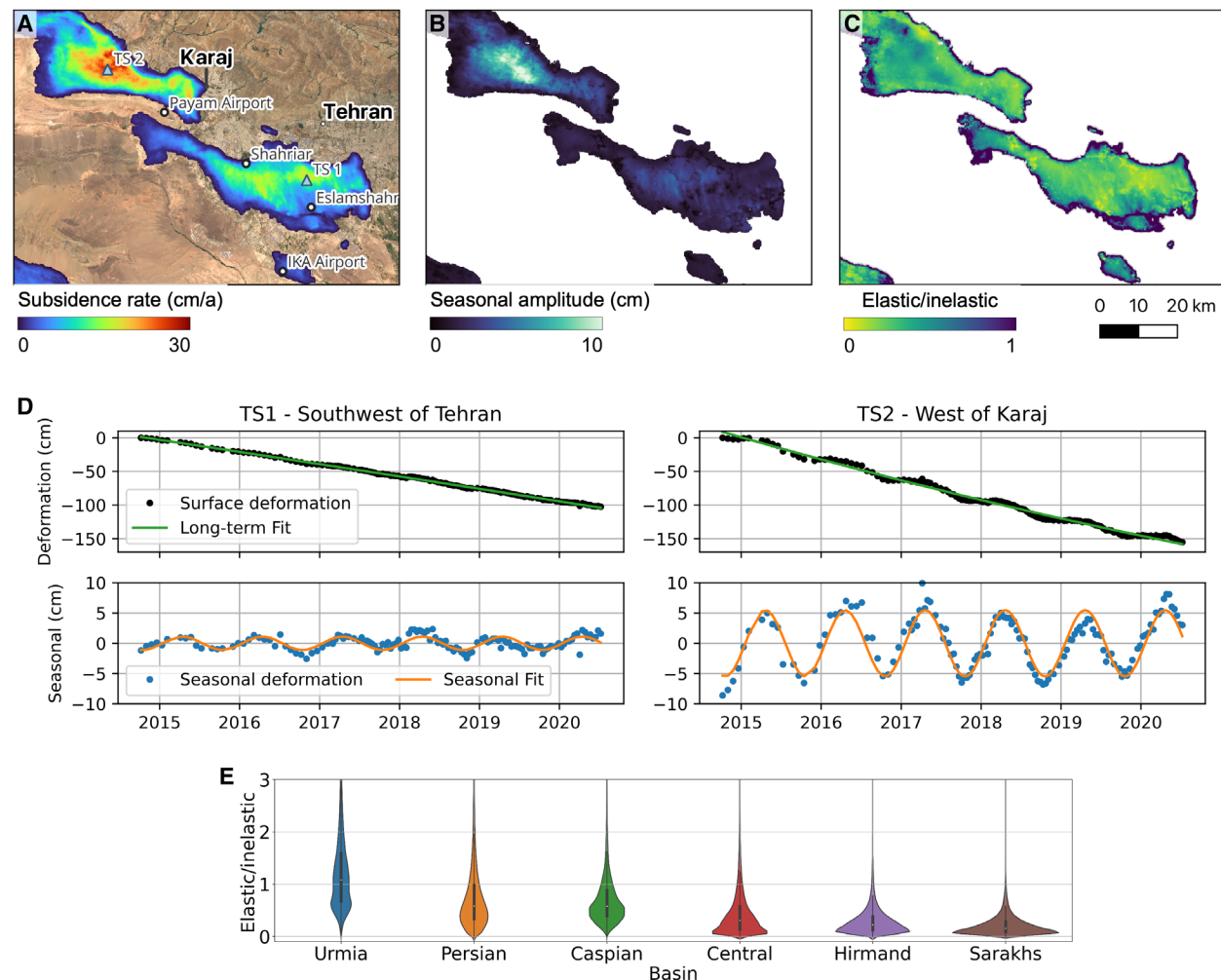


Fig. 3. Elastic/inelastic ratio of deformation as a proxy for groundwater extraction sustainability. (A) Estimated long-term subsidence rate, regarded as inelastic deformation, in the area to the southwest of Tehran and Karaj. (B) Estimated peak-to-peak amplitude of the seasonal surface deformation component in the same area, considered as elastic deformation. (C) Ratio between the long-term subsidence, occurring, on average, over 1 year, and the seasonal component. (D) Surface deformation time series for two example points, TS1 and TS2, which experience the highest observed subsidence rates in the vicinities of Tehran and Karaj, respectively, and their seasonal deformation component. The negative values in the time series correspond to subsidence and positive values correspond to uplift. (E) Distribution of elastic/inelastic ratio across different Iranian basins. Please refer to Fig. 1A for the outlines of the basins. Detailed plots for sub-basins are available fig. S4. All analyses are based on the projection of satellite line-of-sight measurements into the vertical direction. The background in (A) is a true color composite of Sentinel-2.

To assess the sustainability of groundwater extraction in various basins, we aggregated the elastic/inelastic ratio to the major basins and sub-basins nationwide. The results in Fig. 3 show that the Urmia, Persian Gulf, and Caspian Sea basins have higher ratios than other basins, attributed to higher annual precipitation facilitating aquifer recharge. In contrast, Central Plateau, Sarakhs, and Hirmand basins exhibited elastic/inelastic ratios distributed close to zero, indicating highly unsustainable groundwater extraction in these areas. The sub-basin level analysis provided a clearer distribution of unsustainable hot spots (results in fig. S4). Sub-basins in the eastern part of the country generally exhibited lower elastic/inelastic ratios, indicating highly unsustainable groundwater extraction practices. In contrast, the situation appears more favorable in the north, northwest, and southwest regions, where sub-basins show higher ratios of elastic/inelastic. This favorable trend is likely due to higher precipitation in

these basins compared to the central, eastern, and southern regions, offering greater potential for aquifer recharge.

Agriculture as the primary user of groundwater

Our analysis provides convincing evidence of a substantial association between land subsidence and groundwater extraction for irrigation. While less than 4% of land subsidence occurs in built-up areas, more than two-thirds of subsiding lands are classified as agriculture in the Copernicus Global Land Service (24), and almost 40% of land subsidence occurs in irrigated lands in the Global Food Security-support Analysis Data (25). Furthermore, nearly half of the annual total groundwater loss, amounting to 840 MCM, occurs in irrigated lands. This highlights the critical role of agriculture in groundwater depletion.

A comparison between estimated groundwater loss and official statistics of irrigated crops and orchards published in 2019 by the

Ministry of Agriculture of Iran (26, 27) shows different relationships between agricultural production and groundwater depletion (Fig. 4). Although most provinces have larger areas of rainfed than irrigated agriculture, irrigated lands contribute to the majority of agricultural products. The highest agricultural production occurs in Khuzestan with 13%, followed by Fars with 10%, and Kerman, Khorasan Razavi, and Mazandaran, each with 6%. However, due to large surface water availability, Khuzestan and Mazandaran are responsible for only 3% and 0.1% of total groundwater loss, respectively. In contrast, Khorasan Razavi, Kerman, and Fars are responsible for 22%, 19%, and 8% of total groundwater depletion. These findings underscore a pronounced disparity between groundwater consumption and agricultural production in different provinces of Iran, revealing that high pumping rates do not always correspond to equally high production levels. However, it is clear that current rates of groundwater depletion pose a severe threat to future agricultural production in most Iranian provinces.

Impact of land subsidence on the population and infrastructure

This study reveals a considerable impact of land subsidence on Iran's population (Fig. 5). Approximately 14 million people, more than one-fifth of the population live in areas directly affected by substantial

subsidence. Risk analysis using population data and subsidence measurements indicates that around 7% of the population (about 5.6 million individuals) reside in low-risk areas, 10% (approximately 7.7 million) in medium-risk areas, and 1% (0.9 million) in high-risk areas. Provinces such as Kerman, Alborz, Khorasan Razavi, Isfahan, and Tehran have more than a quarter of their population living in subsidence risk. Notably, more than 95% of the high subsidence risk population is concentrated in Tehran, Alborz, Fars, Khorasan Razavi, and Kerman, which host 30 million people together. The population residing in high subsidence risk for the mentioned provinces are approximately 350,000, 290,000, 91,000, 89,000, and 52,000, respectively. Moreover, Tehran has more than 3 million people living in medium and low subsidence risk, Khorasan Razavi has more than 2 million, and Kerman has approximately 1.4 million in medium and low-risk areas. Similarly, Alborz has more than 750,000, and Fars has about 600,000 people in medium and low-risk areas.

Subsidence poses a substantial hazard to linear infrastructure across Iran, as revealed by analyzing linear infrastructure data obtained from OpenStreetMap. The study includes metro lines, motorways, primary roads, railway lines, and trunk roads, indicating that a considerable portion of these infrastructure elements pass through subsidence zones. Notably, the railway lines, extending 9500 km, have approximately 1380 km (15%) at subsidence zones, including

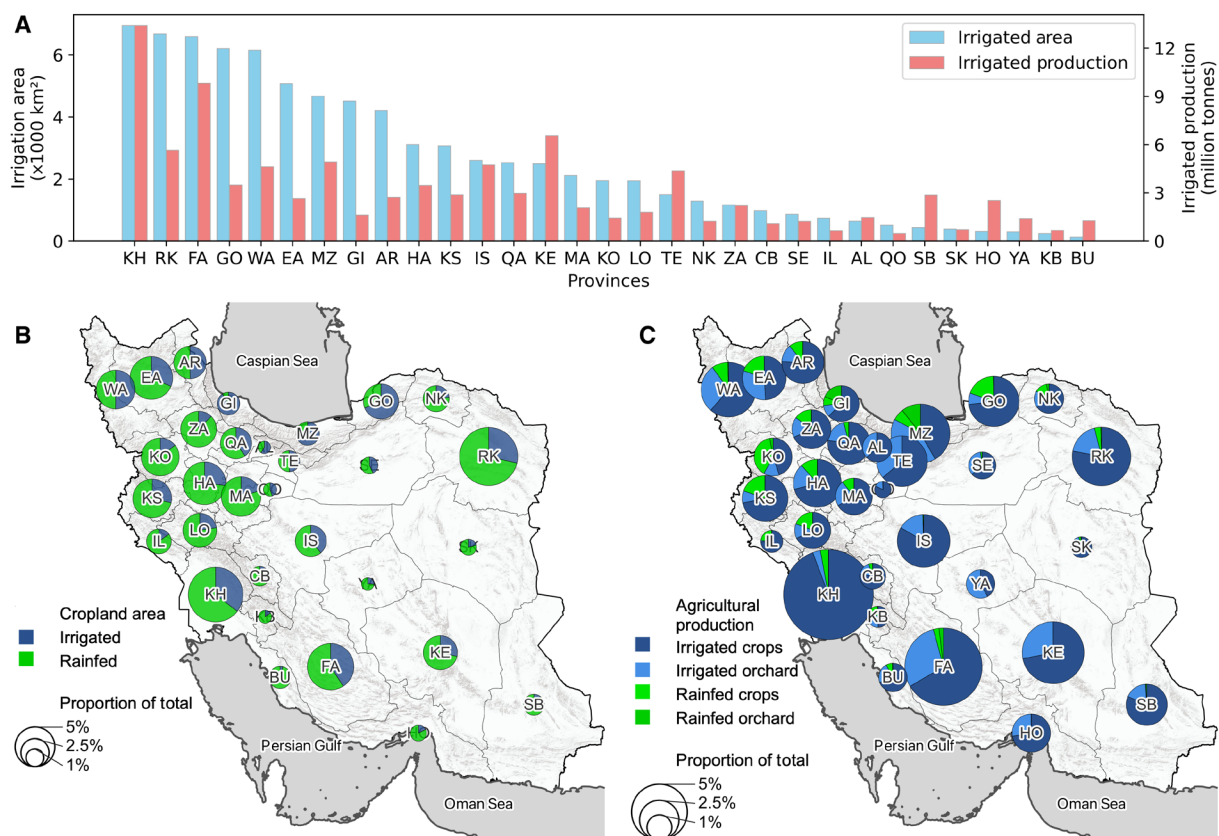


Fig. 4. Cropland types and agricultural production of different provinces across Iran. (A) Total area of irrigated lands and total agricultural production of each province. (B) Share of irrigated and rainfed agricultural areas in different provinces. (C) Share of irrigated and rainfed productions of crops and orchards in different provinces. The information on agricultural areas is based on the Global Food-and-Water Security-support Analysis Data (GFSAD) data (25) and Copernicus Global Land Service (24). The agricultural production information is based on the Ministry of Agriculture of Iran (26, 27). The province names are abbreviated for simplicity. Please refer to Fig. 2A for the full names.

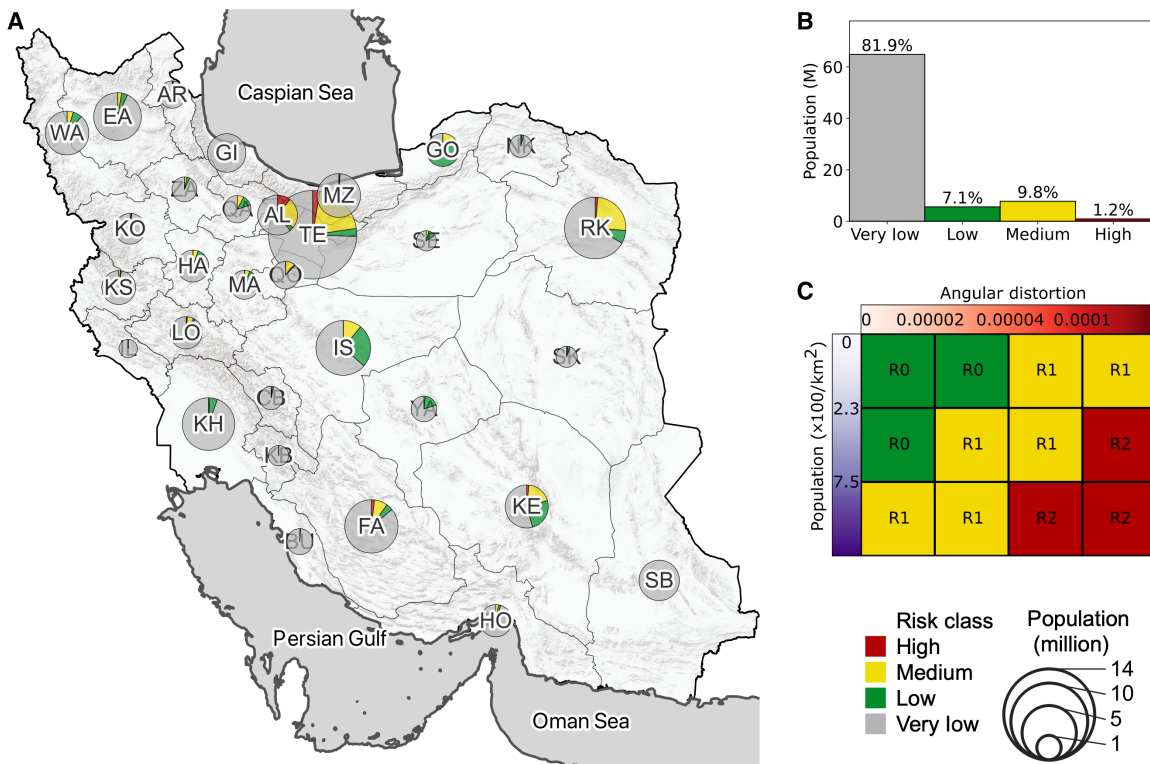


Fig. 5. Risk of subsidence to the population in Iran. (A) Pie charts show the share of the people in each province subject to different subsidence risk classes. The areas of the circles correspond to the total population of each province. (B) Share of the country's population subject to different subsidence risk classes. (C) Risk matrix used to calculate the risk of subsidence to the population. R0 to R2 correspond to low- to high-risk classes. Angular distortion values are calculated from the annual average subsidence.

segments of the busy Tehran-Garmsar and Garmsar-Mashhad lines that connect Tehran to Mashhad. Metro lines in various cities in Iran are also subject to land subsidence, with four of seven metro lines in Tehran and the only metro line in Isfahan running through subsidence areas. The country's total length of metro lines is approximately 370 km, with 55 km (15%) passing through subsidence areas. Moreover, the motorways, spanning about 5100 km, have 580 km (11%) through subsidence regions. Lastly, primary roads (approximately 36,600 km) have 3550 km (10%) and trunk roads (about 34,000 km) have 4300 km (13%) in subsidence zones.

Other infrastructures, including airports, metro stations, and railway stations, in Iran are at considerable risk of subsidence. Eight of the 61 large and medium-sized airports are located in subsidence zones, including the Tehran International Airport, with more than 8 million annual passengers. The Isfahan and Urmia international airports are also affected, as well as Kerman, Gorgan, and Shahrood, which are national civil airports located in subsidence areas. In addition, 54 of the 310 railway stations, including 14 on the Tehran-Garmsar and Garmsar-Mashhad lines, and 25 of the 215 metro stations, including 14 on the Tehran metro lines and 11 on the Isfahan metro, are located in subsidence zones.

DISCUSSION

Our findings align with previous studies that focused on identifying land subsidence in specific aquifers across Iran, mainly using space technologies (13–15, 28–34). However, it goes beyond existing

knowledge by offering a comprehensive nationwide perspective, revealing that, apart from certain regions such as the mountains in the north and west and the deserts in the center and east, groundwater depletion affects other areas of the country to a large extent. This poses a major threat to water resources, population, and infrastructure, jeopardizing the country's sustainable development. The estimated annual groundwater loss of 1.7 BCM from confined and semiconfined aquifers, comparable to the maximum capacity of the five dams supplying Tehran with water, is alarming. This underscores the severity of groundwater depletion, which can have profound consequences for various sectors. Urgent action is imperative to address this critical issue and safeguard the future well-being of Iran's water resources.

Our estimation of groundwater loss adds valuable information to already available independent estimations from GRACE (10) and in situ data (7). The GRACE mission estimated total water storage loss, including both surface and groundwater, with the Central Desert and Salt Lake catchments having the largest shares, noting 1.8 and 1 BCM of an annual loss, respectively. Our results reveal that less than half of these values are from groundwater loss in each of the two catchments, emphasizing the considerable impact of groundwater deficit. Compared to in situ data (7), our results provide an up-to-date estimation with uniform quality across the country. For instance, while the in situ data suggested that the Gharesu-Gorgan sub-basin only had a depletion rate of 0.001 BCM per year, our data revealed that this basin had a groundwater depletion rate of 0.14 BCM per year. The comprehensive, up-to-date, and medium-resolution data on

groundwater loss provided in this study enable a deeper understanding of the groundwater depletion issue and facilitate more effective and informed groundwater management strategies for sustainable water resource planning.

While the agriculture sector is the primary user of groundwater, it is a large economic sector using 17% of Iran's population and contributing 10% to the country's gross domestic product (GDP) (35). However, inefficient irrigation practices and low efficiency resulted in unsustainable groundwater pumping and degraded water resources. Land subsidence associated with groundwater depletion has severe consequences for communities and undermines other economic sectors in Iran. Tehran province, which accounts for more than 20% of Iran's GDP, primarily through services and industry sectors, has a relatively small contribution from agriculture, representing only 2% of the province's gross value added. However, even this small contribution of agriculture is at the cost of major subsidence risk to the population and infrastructure, which could undermine Tehran's economy in the long term.

Given the increasing climate variability, including frequent droughts and floods, water availability for agriculture becomes uncertain. For instance, the 2019 Khuzestan flood, followed by a drought in 2021, further emphasizes this uncertainty. In such a context, groundwater will be crucial for future agriculture and food security (36, 37). Therefore, urgent remedies are essential to ensure sustainable irrigation practices and avoid escalating pressure on groundwater resources (2, 11). Failure to implement measures that promote efficient irrigation practices and responsible groundwater management not only threatens the livelihoods of communities dependent on agriculture but also poses a substantial risk to critical economic sectors, such as transportation and urban infrastructure.

Over the past six decades, rapid industrial and agricultural development, along with a quadrupling population, has largely increased water demand in Iran. Groundwater extraction rates are now twice the sustainable levels (6), with deep wells contributing to groundwater depletion. Only half of the country's groundwater yield comes from sustainable sources such as springs and Qanats, a sustainable underground system to transfer groundwater from the mountain feet to the central parts of Iran. The remaining half is taken from deep wells, based on data from Iran water resource management company (<https://www.wrm.ir>). The country's irrigation efficiency is below 35%, with pressurized water used in less than 5% of irrigated lands (38). To address the groundwater problem, efficient water management policies are crucial, including enforcing regulations for more efficient irrigation practices and limiting groundwater pumping. In addition, implementing land-use planning in agricultural areas, closely monitoring irrigated crops, and imposing zoning regulations to restrict agricultural activities in subsidence-prone regions are effective measures to mitigate groundwater depletion. While some temporary solutions such as water transfer from the Persian Gulf basin have been implemented, they do not resolve downstream water scarcity issues and may exacerbate conflicts between local communities (39).

In conclusion, our study highlights the urgent need for action to address the critical issue of groundwater depletion in Iran and underlines the importance of recognizing the groundwater crisis as a nationwide issue. The use of remote sensing data has provided consistent results, aiding policymakers and communities in comprehending the nationwide problem at a fine scale. Addressing the groundwater issue is an urgent and critical task to secure Iran's water resources for the

future and ensure water security for its population and various economic sectors.

Note that our analysis has certain limitations due to the assumptions made during estimations. First, we estimate subsidence by projecting satellite line-of-sight measurements into vertical, assuming that horizontal displacement is negligible. Previous studies indicate that the primary deformation component in local aquifers, such as Tehran and Rafsanjan, is vertical (13, 14). Nevertheless, more reliable estimates can be obtained by using both ascending and descending geometries. Second, we assume that the observed subsidence is due to the compression of confined and semiconfined aquifers. Hence, our estimation cannot provide information about unconfined aquifers. Combination of our estimations with GRACE observations, which cannot differentiate between confined and unconfined water loss, will provide a complete picture of the groundwater situation in Iran.

Another aspect to consider about our results is that our classification of subsidence hazard and population density into different classes, using Jenks Natural Breaks, is solely based on statistically significant breakpoints in data distribution. As a result, it does not incorporate any explicit physical meaning (40). This approach provides an overall picture of the subsidence hazard and risk across the country. However, at local scales, it is necessary to consider geological and geotechnical parameters, which exhibit considerable variability across different regions, to obtain a more accurate assessment of subsidence risk.

The importance of our research extends beyond Iran's borders. The issue of groundwater depletion (41, 42) and land subsidence (43–46) has become a growing global concern. Two-thirds of the world's population, spanning various nations and regions, grapple with water scarcity for at least 1 month a year (47). Consequently, the unsustainable utilization of groundwater resources and related subsidence is not unique to Iran; it resonates as a global challenge (5, 48–54). The consequences are stark and immediate. Diminishing water tables, shrinking lakes, and disappearing wetlands are signals of water stress experienced in numerous parts of the world (55). Extending similar assessments throughout water-stressed regions can enhance understanding of the regional water crisis and facilitate sustainable water resource management. Moreover, as the use of machine learning and deep learning becomes more common in studying land subsidence and groundwater depletion, our data can additionally serve as training data to improve the reliability of these models (17, 18, 56).

MATERIALS AND METHODS

InSAR processing

This study used Synthetic Aperture Radar (SAR) data from Sentinel-1 satellites acquired in 10 descending tracks from 2014 to 2020 and performed a modified small baseline method (57, 58) to estimate the time series of surface deformation across Iran. We processed a total of more than 6000 scenes of data. Figure S1 illustrates the coverage of different frames of Sentinel-1 across Iran. We obtained the data from the Alaska Satellite Facility in Single Look Complex (SLC) format. For each data track, we concatenated all frames acquired on the same date to form long SLC images covering the country from north to south. Then, we selected one date in each track as the reference and coregistered and resampled all other images to the reference image.

After that, we formed a network of interferograms, similar to a small baseline network (57), using an ideal temporal baseline of 60 days, and connected each image to the two images closest to the ideal baseline. We multilooked the interferograms by factors of 10×2

in image range and azimuth directions, respectively. We used precise orbital data and Shuttle Radar Topography Mission (SRTM) Digital Elevation Model (DEM) (59) to remove the geometric and topographic phase components, respectively. Afterward, we filtered the interferograms using adaptive filtering and unwrapped them using the minimum cost flow (60) method. After the unwrapping, we downsampled the unwrapped interferograms by a factor of 2×2 , which corresponds to approximately 100 m by 100 m on the ground. We conducted the interferometric processing in the GAMMA Software (61). Finally, we inverted the network of interferograms to estimate the phase change time series, which are mainly composed of surface deformation and tropospheric phase delay.

Containing tropospheric phase delay

To obtain surface deformation from the time series, nondeformation phase changes, particularly from tropospheric phase delay, should be estimated and removed. Furthermore, in extensive interferograms such as those used in this study, selecting a unique reference point is impossible as deformation areas are distributed across different regions. Therefore, we estimate a correction surface for each date that jointly accounts for tropospheric phase delay and reference area. The correction surface is empirically calculated by interpolating p_1 and p_2 parameters estimated from 25 km-by-25 km patches using Eq. 1

$$c_{ik} = p_1^k + p_2^k(h_i - h_0^k) \quad (1)$$

where h_i is the ground elevation of the pixel i , h_0^k is the minimum elevation of pixels in patch k , and c_{ik} is the correction estimated for the pixel. The parameter p_1 accounts for the reference phase and broad-scale tropospheric phase delay and p_2 for the stratified tropospheric phase delays correlated with topography. Estimating parameters for individual patches allows for considering the spatial variations of the troposphere, and the parameters are then interpolated to form a continuous surface. However, any deformation phase biases the estimation of parameters in this method. Therefore, we adopt an iterative approach to estimate an average velocity and mask out areas with absolute deformation higher than 1 cm/year. After that, we performed a dilation operation with a kernel size of 9×9 to expand the mask areas to low-magnitude deformation.

Estimating deformation components

To model the subsidence signal, we assume that it consists of a long-term trend, acceleration, and seasonal variation. We use a quadratic polynomial and a seasonal component to find the best-fit model for the time series $X(t)$ as a function of time t .

$$X(t) = \beta_1 + \beta_2 t + \beta_3 t^2 + \beta_4 \sin\left(\frac{2\pi}{365}t\right) + \beta_5 \cos\left(\frac{2\pi}{365}t\right) + \epsilon \quad (2)$$

Here, β represents the parameters of the model and ϵ is the model bias and/or data error. We estimate the amplitude of the seasonal signal A and its delay τ as follows

$$A = \sqrt{\beta_4^2 + \beta_5^2} \quad (3)$$

$$\tau = \frac{365}{2\pi} \tan^{-1}(\beta_4 / \beta_5) \quad (4)$$

After calculating different deformation components in each track of Sentinel-1 data, we project the results from the satellite line-of-sight

to the vertical direction, assuming that the horizontal component of deformation is one order of magnitude smaller than the vertical component, as reported in other studies (13, 14), and therefore is negligible. Last, we geocode and mosaic the results to create a nationwide map for each component.

Pinpointing subsidence zones

Using the nationwide velocity map and several auxiliary data, we could detect anomalies in InSAR average velocity associated with land subsidence. First, we identified permanent and temporal water bodies using the Copernicus Global Land Service (24) and eliminated these areas. Second, as land subsidence primarily occurs in plains with gentle topography variations, we created a mask of areas with slopes larger than 5% using a slope map estimated from SRTM DEM (59). In addition, we applied an opening operation with a 5×5 kernel size to ensure that local slopes caused by minor topographic variations did not mask relatively flat areas. Furthermore, we used the United States Geological Survey earthquake catalog to locate major tectonic events with a magnitude greater than M5 and excluded them from the subsidence candidates.

Estimating the groundwater loss

We estimate the volume of extracted groundwater using InSAR subsidence measurements as suggested in (62). Subsidence can occur due to consolidation in unconfined and confined aquifers. However, in confined aquifers, subsidence is typically more prominent due to higher compaction of weaker sediments such as clay. For a confined aquifer system, the change in the volume of water, or the aquifer storage, is directly proportional to the head change Δh

$$\Delta S = S_s b A \Delta h \quad (5)$$

where b is the aquifer system thickness and A is the area of the aquifer.

S_s is the specific storage corresponding to the volume of water released from a confined unit-area column of soil and per unit decline of water level. The specific storage is the sum of skeletal-specific storage, S_{SK} , due to the compressibility of the aquitard, and water-specific storage, S_{SW} , corresponding to the compressibility of water (12). The latter is typically one to three orders of magnitude smaller, and hence, we neglect it.

$$S_s = S_{SK} \quad (6)$$

S_{SK} is related to Δb , the compaction of the aquifer, which is measured as land subsidence with the following equation

$$S_{SK} = \frac{\Delta b}{b \Delta h} \quad (7)$$

Using Eqs. 5 to 7, the volume of extracted groundwater from the confined aquifer compaction, ΔS , can be estimated as

$$\Delta S = A \Delta b \quad (8)$$

It should be noted that this estimation is a lower bound value of groundwater released from confined and semiconfined aquifers due to consolidation of aquifer matrix. The total amount of groundwater released from the aquifer might be considerably higher, as the specific yield can be two to three orders of magnitude larger than the specific storage.

Subsidence hazard and risk analysis

We estimate the subsidence risk to the population by evaluating the differential settlement instead of the subsidence magnitude. To this

end, we utilize angular distortion, β , which has been suggested in previous studies as a critical parameter for determining subsidence hazard (50).

$$\beta = \frac{\delta b}{L} \quad (9)$$

The maximum differential subsidence, δb , between a point and its neighboring points, is divided by the distance, L , between them to obtain the value of angular distortion. Higher values of angular distortion indicate a higher probability of structural damage. We estimate angular distortion using the average rate of subsidence estimated by InSAR observations.

We use the population density as a proxy for building density to estimate the subsidence risk to them. For a regular grid, we assign the risk level to each pixel based on angular distortion and population density data. The risk matrix (63) associates different risk classes to different pixels based on hazards and vulnerability levels, with the Jenks natural breaks clustering the population density and angular distortion into three levels (40). We assign the pixels outside the subsidence areas to the very low-risk group. Note that the Jenks natural breaks method does not incorporate explicit physical meanings or geotechnical principles into the classification; it rather identifies the most statistically significant breakpoints in data distribution.

We used both vector and raster population data to analyze the population distribution in Iran and the impact of land subsidence on them. We obtained the vector data by extracting the boundaries of the 429 counties in Iran and the 22 districts of Tehran from OpenStreetMap. We assigned the population data to each county based on the 2016 Census conducted by the Statistical Centre of Iran, which provides information on the urban and rural populations. To assign the population to a 100-m grid, we first applied a built-up area mask from the Copernicus Global Land Service (24) to exclude non-built-up areas. We then used the built-up fraction estimation at a spatial resolution of 100 m as a weight to assign the population of each county to a 100-m grid. Last, we estimated the population density for the raster data.

Supplementary Materials

This PDF file includes:

Figs. S1 to S4

REFERENCES AND NOTES

1. K. Madani, A. AghaKouchak, A. Mirchi, Iran's socio-economic drought: Challenges of a water-bankrupt nation. *Iran. Stud.* **49**, 997–1016 (2016).
2. B. Jaleh, M. Eslamipanah, Restore Iran's declining groundwater. *Science* **379**, 148–148 (2023).
3. M. Rodell, J. S. Famiglietti, D. N. Wiese, J. T. Reager, H. K. Beaudoin, F. W. Landerer, M.-H. Lo, Emerging trends in global freshwater availability. *Nature* **557**, 651–659 (2018).
4. C. Herbert, P. Döll, Global assessment of current and future groundwater stress with a focus on transboundary aquifers. *Water Resour. Res.* **55**, 4760–4784 (2019).
5. G. Herrera-García, P. Ezquerro, R. Tomás, M. Béjar-Pizarro, J. López-Vinieles, M. Rossi, R. M. Mateos, D. Carreón-Freyre, J. Lambert, P. Teatini, E. Cabral-Cano, G. Erkens, D. Galloway, W.-C. Hung, N. Kakar, M. Sneed, L. Tosi, H. Wang, S. Ye, Mapping the global threat of land subsidence. *Science* **371**, 34–36 (2021).
6. Y. Wada, L. P. H. van Beek, M. F. P. Bierkens, Nonsustainable groundwater sustaining irrigation: A global assessment. *Water Resour. Res.* **48**, W00L06 (2012).
7. S. Ashraf, A. Nazemi, A. AghaKouchak, Anthropogenic drought dominates groundwater depletion in Iran. *Sci. Rep.* **11**, 9135 (2021).
8. E. Forootan, R. Rietbroek, J. Kusche, M. A. Sharifi, J. L. Awange, M. Schmidt, P. Omondi, J. Famiglietti, Separation of large scale water storage patterns over Iran using GRACE, altimetry and hydrological data. *Remote Sens. Environ.* **140**, 580–595 (2014).
9. M. Khaki, E. Forootan, M. Kuhn, J. Awange, A. I. J. M. van Dijk, M. Schumacher, M. A. Sharifi, Determining water storage depletion within Iran by assimilating GRACE data into the W3RA hydrological model. *Adv. Water Resour.* **114**, 1–18 (2018).
10. P. Saemian, M. J. Tourian, A. AghaKouchak, K. Madani, N. Sneeuw, How much water did Iran lose over the last two decades? *J. Hydrol. Reg. Stud.* **41**, 101095 (2022).
11. M. Negahdary, Shrinking aquifers and land subsidence in Iran. *Science* **376**, 1279–1279 (2022).
12. R. G. Smith, R. Knight, J. Chen, J. A. Reeves, H. A. Zebker, T. Farr, Z. Liu, Estimating the permanent loss of groundwater storage in the southern San Joaquin Valley, California. *Water Resour. Res.* **53**, 2133–2148 (2017).
13. M. Haghshenas Haghighi, M. Motagh, Ground surface response to continuous compaction of aquifer system in Tehran, Iran: Results from a long-term multi-sensor InSAR analysis. *Remote Sens. Environ.* **221**, 534–550 (2019).
14. M. Motagh, R. Shamshiri, M. Haghshenas Haghighi, H.-U. Wetzel, B. Akbari, H. Nahavandchi, S. Roessner, S. Arabi, Quantifying groundwater exploitation induced subsidence in the Rafsanjan plain, southeastern Iran, using InSAR time-series and in situ measurements. *Eng. Geol.* **218**, 134–151 (2017).
15. M. Motagh, Y. Djamar, T. R. Walter, H.-U. Wetzel, J. Zschau, S. Arabi, Land subsidence in Mashhad Valley, northeast Iran: Results from InSAR, levelling and GPS. *Geophys. J. Int.* **168**, 518–526 (2007).
16. M. Haghshenas Haghighi, M. Motagh, Land subsidence hazard in Iran revealed by country-scale analysis of Sentinel-1 InSAR, in *The International Archives of the Photogrammetry, Remote Sensing and Spatial Information Sciences* (2021), vol. XLIII-B3-2021, pp. 155–161.
17. M. Panahi, K. Khosravi, A. Golkarian, M. Roostaei, R. Barzegar, E. Omidvar, F. Rezaie, P. M. Saco, A. Sharifi, C. Jun, S. M. Bateni, C.-W. Lee, S. Lee, A country-wide assessment of Iran's land subsidence susceptibility using satellite-based InSAR and machine learning. *Geocarto Int.* **37**, 14065–14087 (2022).
18. M. F. Hasan, R. Smith, S. Vajedian, R. Pommerenke, S. Majumdar, Global land subsidence mapping reveals widespread loss of aquifer storage capacity. *Nat. Commun.* **14**, 6180 (2023).
19. A. Haghipour, A. Aghanabati, Geological map of Iran, scale 1:2,500,000 (Geological Survey of Iran, 1985).
20. R. M. Pollastro, F. Persits, D. W. Steinhouser, Surficial geology of Iran (geo2cg) (U.S. Geological Survey data release, 1999); <https://doi.org/10.5066/P93ZEPFY>.
21. J. D. Pelletier, P. D. Broxton, P. Hazenberg, X. Zeng, P. A. Troch, G. Niu, Z. C. Williams, M. A. Brunke, D. Gochis, Global 1-km gridded thickness of soil, regolith, and sedimentary deposit layers (ORNL DAAC, 2016).
22. R. Noori, M. Maghrebi, S. Jessen, S. M. Bateni, E. Heggy, S. Javadi, M. Noury, S. Pistre, S. Abolfathi, A. AghaKouchak, Decline in Iran's groundwater recharge. *Nat. Commun.* **14**, 6674 (2023).
23. M. Bockstiegel, J. C. Richard-Cerda, E. Muñoz-Vega, M. H. Haghighi, M. Motagh, R. Lalehzari, S. Schulz, Simulation of present and future land subsidence in the Rafsanjan plain, Iran, due to groundwater overexploitation using numerical modeling and InSAR data analysis. *Hydrogeol. J.* **32**, 289–305 (2024).
24. M. Buchhorn, B. Smets, L. Bertels, B. D. Roo, M. Lesiv, N.-E. Tsednbazar, M. Herold, S. Fritz, Copernicus global land service: Land cover 100m: Collection 3: Epoch 2019: Globe, (Zenodo, 2020); <https://doi.org/10.5281/zenodo.3939050>.
25. P. Teluguntla, P. Thenkabail, A. Oliphant, M. Gumma, I. Aneece, D. Foley, R. McCormick, Landsat-derived global rainfed and irrigated-cropland product 30 m v001 (NASA EOSDIS Land Processes DAAC, 2023); <https://doi.org/10.5067/COMMUNITY/LGRIP/LGRIP30.001>.
26. K. Ahmadi, H. Ebazdadeh, F. Hatami, R. Hosseinpour, H. Abdshah, Yearbook of Agricultural Statistics, Year 2019 - Volume III, Orchards (Ministry of Agriculture of Iran, 2020).
27. K. Ahmadi, H. Ebazdadeh, F. Hatami, H. Abdshah, A. Kazemian, Yearbook of Agricultural Statistics, Water Year 2018–2019 - Volume I, Crops (Ministry of Agriculture of Iran, 2020).
28. S. M. Mousavi, A. Shamsai, M. H. E. Naggar, M. Khamehchian, A GPS-based monitoring program of land subsidence due to groundwater withdrawal in Iran. *Can. J. Civ. Eng.* **28**, 452–464 (2001).
29. J. Anderssohn, H.-U. Wetzel, T. R. Walter, M. Motagh, Y. Djamar, H. Kaufmann, Land subsidence pattern controlled by old alpine basement faults in the Kashmar Valley, Northeast Iran: Results from InSAR and levelling. *Geophys. J. Int.* **174**, 287–294 (2008).
30. M. Motagh, T. R. Walter, M. A. Sharifi, E. Fielding, A. Schenk, J. Anderssohn, J. Zschau, Land subsidence in Iran caused by widespread water reservoir overexploitation. *Geophys. Res. Lett.* **35**, L16403 (2008).
31. M. Dehghani, M. J. Valadan Zanj, I. Entezam, A. Mansourian, S. Saatchi, InSAR monitoring of progressive land subsidence in Neyshabur, Northeast Iran. *Geophys. J. Int.* **178**, 47–56 (2009).
32. M. Amighpey, S. Arabi, Studying land subsidence in Yazd province, Iran, by integration of InSAR and levelling measurements. *Remote Sens. Appl. Soc. Environ.* **4**, 1–8 (2016).
33. A. Ghazifard, A. Moslehi, H. Safaei, M. Roostaei, Effects of groundwater withdrawal on land subsidence in Kashan Plain, Iran. *Bull. Eng. Geol. Environ.* **75**, 1157–1168 (2016).

34. S. Karimzadeh, Characterization of land subsidence in Tabriz basin (NW Iran) using InSAR and watershed analyses. *Acta Geod. Geophys.* **51**, 181–195 (2016).
35. Central Bank of the Islamic Republic of Iran, *Annual economic report and balance sheet 2018* (Central Bank of the Islamic Republic of Iran, Tehran, 2020); www.cbi.ir/page/24428.aspx.
36. R. G. Taylor, B. Scanlon, P. Döll, M. Rodell, R. van Beek, Y. Wada, L. Longuevergne, M. Leblanc, J. S. Famiglietti, M. Edmunds, L. Konikow, T. R. Green, J. Chen, M. Taniguchi, M. F. P. Bierkens, A. MacDonald, Y. Fan, R. M. Maxwell, Y. Yechieli, J. J. Gurdak, D. M. Allen, M. Shamsudduha, K. Hiscock, P. J.-F. Yeh, I. Holman, H. Treidel, Ground water and climate change. *Nat. Clim. Change* **3**, 322–329 (2013).
37. B. R. Scanlon, S. Fakhreddine, A. Rateb, I. de Graaf, J. Famiglietti, T. Gleeson, R. Q. Grafton, E. Jobbagy, S. Kebede, S. R. Kolusu, L. F. Konikow, D. Long, M. Mekonnen, H. M. Schmied, A. Mukherjee, A. MacDonald, R. C. Reedy, M. Shamsudduha, C. T. Simmons, A. Sun, R. G. Taylor, K. G. Villholth, C. J. Vörösmarty, C. Zheng, Global water resources and the role of groundwater in a resilient water future. *Nat. Rev. Earth Environ.* **4**, 87–101 (2023).
38. K. Madani, Water management in Iran: What is causing the looming crisis? *J. Environ. Stud. Sci.* **4**, 315–328 (2014).
39. D. Michel, Iran's impending water crisis, in *Water, Security and U.S. Foreign Policy* (Routledge, 2017).
40. G. F. Jenks, The data model concept in statistical mapping. *Int. Yearb. Cartogr.* **7**, 186–190 (1967).
41. S. Jasechko, H. Seybold, D. Perrone, Y. Fan, M. Shamsudduha, R. G. Taylor, O. Fallatah, J. W. Kirchner, Rapid groundwater decline and some cases of recovery in aquifers globally. *Nature* **625**, 715–721 (2024).
42. S. Jasechko, D. Perrone, Global groundwater wells at risk of running dry. *Science* **372**, 418–421 (2021).
43. Z. D. Tessler, C. J. Vörösmarty, M. Grossberg, I. Gladkova, H. Aizenman, J. P. M. Syvitski, E. Foufoula-Georgiou, Profiling risk and sustainability in coastal deltas of the world. *Science* **349**, 638–643 (2015).
44. K. D. Murray, R. B. Lohman, Short-lived pause in Central California subsidence after heavy winter precipitation of 2017. *Sci. Adv.* **4**, eaar8144 (2018).
45. P.-C. Wu, M. Wei, S. D'Hondt, Subsidence in coastal cities throughout the world observed by InSAR. *Geophys. Res. Lett.* **49**, e2022GL098477 (2022).
46. L. O. Ohnenhen, M. Shirzaei, C. Ojha, M. L. Kirwan, Hidden vulnerability of US Atlantic coast to sea-level rise due to vertical land motion. *Nat. Commun.* **14**, 2038 (2023).
47. M. M. Mekonnen, A. Y. Hoekstra, Four billion people facing severe water scarcity. *Sci. Adv.* **2**, e1500323 (2016).
48. D. L. Galloway, T. J. Burbey, Review: Regional land subsidence accompanying groundwater extraction. *Hydrogeol. J.* **19**, 1459–1486 (2011).
49. F. Ameling, D. L. Galloway, J. W. Bell, H. A. Zebker, R. J. Lacznak, Sensing the ups and downs of Las Vegas: InSAR reveals structural control of land subsidence and aquifer-system deformation. *Geology* **27**, 483–486 (1999).
50. F. Cigna, D. Tapete, Present-day land subsidence rates, surface faulting hazard and risk in Mexico City with 2014–2020 Sentinel-1 IW InSAR. *Remote Sens. Environ.* **253**, 112161 (2021).
51. M. Bagheri-Gavkosh, S. M. Hosseini, B. Ataie-Ashtiani, Y. Sohani, H. Ebrahimian, F. Morovat, S. Ashrafi, Land subsidence: A global challenge. *Sci. Total Environ.* **778**, 146193 (2021).
52. S. Garg, M. Motagh, J. Indu, V. Karanam, Tracking hidden crisis in India's capital from space: Implications of unsustainable groundwater use. *Sci. Rep.* **12**, 651 (2022).
53. W. Tang, X. Zhao, M. Motagh, G. Bi, J. Li, M. Chen, H. Chen, M. Liao, Land subsidence and rebound in the Taiyuan basin, northern China, in the context of inter-basin water transfer and groundwater management. *Remote Sens. Environ.* **269**, 112792 (2022).
54. M. Peng, Z. Lu, C. Zhao, M. Motagh, L. Bai, B. D. Conway, H. Chen, Mapping land subsidence and aquifer system properties of the Willcox Basin, Arizona, from InSAR observations and independent component analysis. *Remote Sens. Environ.* **271**, 112894 (2022).
55. S. Postel, *The Last Oasis: Facing Water Scarcity* (Earthscan, 1992), vol. 26, pp. 2332–2333.
56. T. Davydzenka, P. Tahmasebi, N. Shokri, Unveiling the global extent of land subsidence: The sinking crisis. *Geophys. Res. Lett.* **51**, e2023GL104497 (2024).
57. P. Berardino, G. Fornaro, R. Lanari, E. Sansosti, A new algorithm for surface deformation monitoring based on small baseline differential SAR interferograms. *IEEE Trans. Geosci. Remote Sens.* **40**, 2375–2383 (2002).
58. Z. Yunjun, H. Fattah, F. Ameling, Small baseline InSAR time series analysis: Unwrapping error correction and noise reduction. *Comput. Geosci.* **133**, 104331 (2019).
59. A. Jarvis, H. I. Reuter, A. Nelson, E. Guevara, Hole-Filled Seamless SRTM Data V4 [International Centre for Tropical Agriculture (CIAT), 2008]; <http://srtm.csi.cgiar.org>.
60. C. W. Chen, H. A. Zebker, Two-dimensional phase unwrapping with use of statistical models for cost functions in nonlinear optimization. *J. Opt. Soc. Am. A. Image Sci. Vis.* **18**, 338–351 (2001).
61. U. Wegmüller, C. Werner, T. Strozzi, A. Wiesmann, O. Frey, M. Santoro, Sentinel-1 support in the GAMMA software. *Procedia Comput. Sci.* **100**, 1305–1312 (2016).
62. R. G. Smith, S. Majumdar, Groundwater storage loss associated with land subsidence in Western United States mapped using machine learning. *Water Resour. Res.* **56**, e2019WR026621 (2020).
63. P. R. Garvey, Z. F. Lansdowne, Risk matrix: An approach for identifying, assessing, and ranking program risks. *Air Force J. Logist.* **22**, 18–21 (1998).

Acknowledgments: This study contains modified Copernicus Sentinel data 2018–2023, processed by European Space Agency. QGIS and Python were used to create the figures. We would like to express our gratitude for the valuable comments from the anonymous reviewers, which considerably improved the original manuscript. We also extend our gratitude to H. Akhani for the valuable insights into land subsidence and water scarcity in Iran. M.M. acknowledges support from the BMBF-funded mobility program, RSGR. **Funding:** The authors acknowledge that they received no funding in support of this research. **Author contributions:** Conceptualization and writing: M.H.H. and M.M. Methodology, investigation, and visualization: M.H.H. **Competing interests:** The authors declare that they have no competing interests. **Data and materials availability:** All data needed to evaluate the conclusions in the paper are present in the paper and/or the Supplementary Materials. The results of this study have been deposited in Zenodo and can be found at <https://doi.org/10.5281/zenodo.10815577>.

Submitted 7 September 2023

Accepted 8 April 2024

Published 10 May 2024

10.1126/sciadv.adk3039